Computational and Applied Mathematics (2021) 40:271
https://doi.org/10.1007/s40314-021-01665-6

A collocation method based on localized radial basis functions with reproducibility for nonlocal diffusion models

Jiashu Lu[1] · **Yufeng Nie**[1]

Received: 19 May 2021 / Revised: 18 August 2021 / Accepted: 27 September 2021 /
Published online: 13 October 2021

Abstract
In this paper, a kind of localized radial basis function-based collocation method with reproducibility has been designed for nonlocal diffusion models. The basic idea of the method is to localize the RBF shape function by a corrected kernel with compact support, and meanwhile make the interpolation function to meet the reproducing conditions by modifying the coefficient contained in such kernel. Three types of nonlocal diffusion problems including constant and singular kernels are solved by our method in numerical experiments, which indicates that our method shows almost the same convergent behavior compared with RBF collocation methods, but it is much better conditioning and more time-efficient. It also overcomes the shortcoming that the RK-enhanced RBF method is not convergent for nonlocal diffusion models.

Keywords Nonlocal diffusion · Collocation method · Reproducing kernel method · Localized radial basis functions

Mathematics Subject Classification 65R20 · 45K05 · 45A05 · 65N35

1 Introduction

Recent developed nonlocal continuum models have been used to describe many phenomenons to overcome limitations of classical models expressed by differential equations. Using the integral-type operators to avoid the explicit application of spatial derivatives, solutions which have singular and anomalous behavior can be involved in the solution space of the nonlocal models. For instance, the peridynamic model introduced by Silling (2000) gives a nonlocal counterpart of continuum mechanics to simulate cracks and their evolution in materials. Besides, nonlocal models can be used to describe a more general stochastic jumping process

Communicated by Cassio Oishi.

✉ Yufeng Nie
yfnie@nwpu.edu.cn

Jiashu Lu
jiashulu@mail.nwpu.edu.cn

[1] Xi'an Key Laboratory of Scientific Computation and Applied Statistics, Northwestern Polytechnical University, Xi'an 710129, Shaanxi, China

than the Brown motion corresponding to normal diffusion (Du et al. 2014). These stochastic jump processes allow for discontinuities and jump behaviors in the sample path, and some special nonlocal diffusion operators can also lead to the fractional diffusion equations corresponding to anomalous diffusion (Metzler and Klafter 2000).

There have been lots of works done on nonlocal diffusion models, including theoretical analysis, numerical methods, and applications. Du et al. (2012) developed a nonlocal calculus framework as a tool to provide a variational analysis for it, and pointed out that nonlocal diffusion models can be seen as a bridge connecting both partial differential models and fractional models. In the light of such a framework, there have been a great number of numerical methods developed for nonlocal models, such as finite-element methods (D'Elta et al. 2020), discontinuous Galerkin (DG) methods (Du et al. 2018; Du and Yin 2018), collocation methods (Pasetto et al. 2019), and Fourier spectral methods (Alali and Albin 2020). These methods can be roughly divided into the following two categories: the one is Galerkin-type methods based on the weak form of the model equation, and the other is collocation methods based on the strong form of the model equation. The Galerkin-type method has a more complete theoretical framework, and the numerical solution has better stability compared with the collocation methods. However, for nonlocal problems, the weak form of equations always appears as a double integral of the function to be solved (quadruple integral for 2D and 6-lay integral for 3D), which leads to expensive computational cost, and it will be difficult to approximate such double integral through numerical quadrature. There are lots of fast algorithms developed to speed up the process of solving nonlocal equations. For example, Wang in Liu et al. (2018) and Du et al. (2019) designed a fast algorithm for matrix-vector multiplication by mining the block-Toeplitz structure of the stiffness matrix corresponding to the nonlocal operators. Zhang and Nie (2020) developed a POD-based fast algorithm to speed up the time iteration. However, even these fast algorithms show great efficiency in solving nonlocal equations, they still do not overcome the essential difficulties in generating nonlocal stiffness matrix. Except for the weak form, one can also solve such nonlocal diffusion models based on strong form, to reduce the computational cost compared with Galerkin-based methods. In fact, the meshfree particle method is frequently used in peridynamic simulation. Therefore, in this work, we mainly focus on the meshfree type discretizations for nonlocal problems based on collocation methods.

Meshfree method based on the radial basis functions (RBFs) has attracted great interest from many researchers due to its exponential convergence for smooth functions in complex geometries (Madych and Nelson 1990). The same convergence has been developed for solving PDE with RBF collocation methods (Hu et al. 2005). However, it usually leads to a full and ill-conditioning discrete system when using RBF interpolation or collocation methods, since they are all global methods. To handle it, many localized schemes have been proposed, such as the RBF partition of unity (PU) scheme (Ali et al. 2015; Perracchione 2018). Based on the RBF-PU scheme, a reproducing kernel (RK) enhanced local RBF collocation method has been developed, and it shows almost the same convergent behavior and lower condition number than global RBF collocation methods (Chen et al. 2008) for the Poisson problem. However, even though the above method introduced a kind of reproducing kernel shape function to localize the RBF shape functions, the interpolation u^h still does not have reproducibility for linear functions in a finite domain. In essential, reproducibility plays a significant role in the convergence and stability in RK-based methods (Liu et al. 1995, 1996). In this paper, we redesigned the reproducing condition to let the final interpolation function u^h have reproducibility for monomials, and then, the RK type localized factor will truly make sense. Numerical tests show that the convergent result of such an improved localized RBF scheme is almost the same as the traditional RBF collocation method, but is better condi-

tioning and has a cheaper computation cost. However, the RK enhanced RBF-PU scheme proposed in Chen et al. (2008) is not convergent for nonlocal diffusion problems.

This paper is organized as follows. In Sect. 2, we introduce the nonlocal diffusion equations with Dirichlet volume constraints and some related theories. In Sect. 3, we present the RBF and localized RBF method, and then, a localized approach is given for RBF to make the interpolation function meets the reproducing condition. In Sect. 4, specific implementation processes and details for solving nonlocal diffusion problems are given. In Sect. 5, numerical examples are given to show the effectiveness of such a scheme. Finally, conclusions are made in Sect. 6.

2 Nonlocal diffusion problem

The notations used in this article are introduced as follows. A point in $\mathbb{R}^{\mathrm{d}}$ is expressed as $\mathbf{x} = (x_1, x_2, ..., x_d)$ where d refers to the spatial dimension. For a given multi-index $\boldsymbol{\alpha} = (\alpha_1, \alpha_2, ..., \alpha_{\mathrm{d}})$, denote $\mathbf{x}^{\boldsymbol{\alpha}} = x_1^{\alpha_1} ... x_{\mathrm{d}}^{\alpha_{\mathrm{d}}}$. Let $\Omega \subset \mathbb{R}^{\mathrm{d}}$ be a bounded, open domain, and define the corresponding interaction domain

$$\Omega_I = \{\mathbf{x} \in \mathbb{R}^{\mathrm{d}} : \mathrm{dist}(\mathbf{x}, \Omega) \leq \delta\},$$

and let $\Omega_\delta = \Omega \cup \Omega_I$. Here, δ is called the ***horizon*** which is used to describe the scope of nonlocal interaction. Consider the following nonlocal boundary value problem with Dirichlet volume constraints:

$$\begin{cases} -\mathcal{L}_\delta u(\mathbf{x}) = f(\mathbf{x}), & \text{for } \mathbf{x} \in \Omega \\ u(\mathbf{x}) = h(\mathbf{x}), & \text{for } \mathbf{x} \in \Omega_I, \end{cases} \tag{1}$$

where $\mathcal{L}_\delta$ is the nonlocal diffusion operator defined as

$$\mathcal{L}_\delta u(\mathbf{x}) = \int_{\Omega_\delta} \rho_\delta(\mathbf{x}, \mathbf{y})(u(\mathbf{y}) - u(\mathbf{x}))d\mathbf{y}, \quad \forall x \in \Omega, \tag{2}$$

where ρ_δ is the nonlocal kernel. We assume that the nonlocal kernel is non-negative and symmetric, and has the following scaling:

$$\rho_\delta(\mathbf{x}, \mathbf{y}) = \frac{1}{\delta^{\mathrm{d}+2}} \rho\left(\frac{||\mathbf{x} - \mathbf{y}||}{\delta}\right), \tag{3}$$

where $\rho(\cdot)$ is a non-negative and non-increasing scalar function supported in a ball of radius 1 about $\mathbf{0}$, and $||\cdot||$ denoting the Euclidean norm. The kernel $\rho_\delta(\cdot)$ is further assumed to have a bounded second-order moment

$$\int_{B_{(\mathbf{x},\delta)}} \rho_\delta(\mathbf{y}, \mathbf{x})||\mathbf{y} - \mathbf{x}||^2 d\mathbf{y} \overset{\mathbf{s}=\frac{\mathbf{y}-\mathbf{x}}{\delta}}{=\!=\!=} \int_{B_{(\mathbf{0},1)}} \rho(||\mathbf{s}||)||\mathbf{s}||^2 d\mathbf{s} = 2\mathrm{d}. \tag{4}$$

3 RBF and reproducing kernal localized RBF Method

3.1 RBF and localized RBF collocation method

RBF method is a kind of meshfree method which works with data on the set of scattered points $\mathbf{S} = \{\mathbf{x}_1, \mathbf{x}_2, ..., \mathbf{x}_{N_s}\} \subset \mathbb{R}^{\mathrm{d}}$. The standard RBF interpolation of a given function $u(\mathbf{x})$

can be described as

$$u^h(\mathbf{x}) = \sum_{I=1}^{N_s} u_I g(||\mathbf{x} - \mathbf{x}_I||), \tag{5}$$

where $||\mathbf{x}||$ is the Euclidean norm. u_I is the interpolation coefficient corresponding to point $\mathbf{x}_I$, and g is the RBF, for example, the frequently used multiquadrics (MQ) RBF (Buhmann 2003)

$$g_I(\mathbf{x}) = (r_I^2 + c^2)^{\mathrm{d}-3/2}, \tag{6}$$

where $r_I = ||\mathbf{x} - \mathbf{x}_I||$, and c is ***shape parameter*** of RBF.

Let $R_{N_s} = u - u^h$, and by defining the distance of points in $\mathbf{S}$

$$H(\mathbf{S}) := \max_{\mathbf{y}_j \in \mathbf{S}} \min_{\mathbf{x}_i \in \mathbf{S}} ||\mathbf{y}_j - \mathbf{x}_i||, \tag{7}$$

then we have the exponential error estimates (Madych and Nelson 1992; Hu et al. 2005)

$$\max_{\Omega} |R_{N_s}| = O(\lambda^{c/\bar{h}}), \tag{8}$$

where $c > 0$ is the shape parameter mentioned above, $N_s > 1$, $0 < \lambda < 1$, and $\bar{h} = H(\mathbf{S})$.

Collocation methods using RBFs for elliptic boundary value problems have been researched in Hu et al. (2005). For readability, we briefly list some results without details.

For Poisson's equation with mixed boundary condition

$$\begin{cases} -\Delta u(\mathbf{x}) = f(\mathbf{x}), & \text{for } \mathbf{x} \in \Omega \\ u_\nu(\mathbf{x}) = q_1(\mathbf{x}), & \text{for } \mathbf{x} \in \partial\Omega_N, \\ (u_\nu + \beta u(\mathbf{x})) = q_2(\mathbf{x}), & \text{for } \mathbf{x} \in \partial\Omega_R, \end{cases} \tag{9}$$

where $\beta > 0$ is a constant, $\partial\Omega = \partial\Omega_N \cup \partial\Omega_R$ and u_ν is the out normal derivative on $\partial\Omega$. Using $u^h(\mathbf{x})$ in (5) as a approximation of $u(\mathbf{x})$, we can obtain the discrete form of (9) at collocation points $\mathbf{T} = \{\mathbf{y}_1, \mathbf{y}_2, ..., \mathbf{y}_{N_p}\}$ as

$$\begin{cases} -\Delta u^h(\mathbf{y}_I) = f(\mathbf{y}_I), & \text{for } \mathbf{y}_I \in \mathbf{T} \cap \Omega \\ u_\nu^h(\mathbf{y}_I) = q_1(\mathbf{y}_I), & \text{for } \mathbf{y}_I \in \mathbf{T} \cap \partial\Omega_N, \\ \left(u_\nu + \beta u^h(\mathbf{y}_I)\right) = q_2(\mathbf{y}_I), & \text{for } \mathbf{y}_I \in \mathbf{T} \cap \partial\Omega_R, \end{cases} \tag{10}$$

with $I = 1, 2, ..., N_p$. Convergence results are given in reference (Hu et al. 2005) as the following lemma:

Lemma 1 *Let $h = H(\mathbf{T})$ is the maximal distance between the collocation points $\mathbf{T}$, and suppose the integration rules corresponding to the collocation method is of order r. If choosing h and N_p to satisfy*

$$h^{r+1} N_p^{r+3} = o(1). \tag{11}$$

Then, the solution of the collocation method for (10) has the following error bound:

$$||u - u^h||_h \le C \left\{ ||R_{N_p}||_{2,\Omega} + ||(R_{N_p})_\nu||_{0,\partial\Omega_N} + ||(R_{N_p})_\nu||_{0,\partial\Omega_R} \right\}, \tag{12}$$

where C is a constant independent on N_s and N_p, $||v||_h$ denoting the norm on the solution space of (9)

$$||v||_h := \left\{ ||v||_{1,\Omega}^2 + ||\Delta v||_{0,\Omega}^2 + ||v_\nu||_{0,\partial\Omega_N}^2 + ||(v_\nu + \beta v)||_{0,\partial\Omega_R}^2 \right\}^{1/2}. \tag{13}$$

However, the RBF interpolation and collocation will lead to low computational efficiency and high condition number as the discrete dimension increases, since it is a kind of global method. To deal with it, the authors in Chen et al. (2008) developed a localized RBF collocation method based on reproducing kernel (RK) shape functions. The main idea is to reconstruct the interpolation u^h by multiplying an RK localized factor

$$u^h(\mathbf{x}) = \sum_{I=1}^{N_s} [\phi_I(\mathbf{x}) g_I(\mathbf{x}) u_I], \tag{14}$$

or more general

$$u^h(\mathbf{x}) = \sum_{I=1}^{N_s} [\phi_I(\mathbf{x}) (a_I + g_I(\mathbf{x}) b_I)], \tag{15}$$

where $\phi_I(\mathbf{x})$ is the RK shape function defined as

$$\phi_I(\mathbf{x}) = \varphi_a(||\mathbf{x} - \mathbf{x}_I||) C(\mathbf{x}; \mathbf{x} - \mathbf{x}_I), \tag{16}$$

where $C(\mathbf{x}; \mathbf{x} - \mathbf{x}_I)$ is called the correction function, which consists of a linear combination of polynomials

$$C(\mathbf{x}; \mathbf{x} - \mathbf{x}_I) = \left[\sum_{|\alpha| \le p} (\mathbf{x} - \mathbf{x}_I)^\alpha q_\alpha(\mathbf{x}) \right], \tag{17}$$

and $\varphi_a(||\mathbf{x} - \mathbf{x}_I||)$ is a kernel function with compact support. Usually, we choose a cubic B-spline function as (see (a) of Fig. 1)

$$\varphi_a(z) = \begin{cases} \frac{2}{3} - 4(\frac{z}{a})^2 + 4(\frac{z}{a})^3 & \text{for } 0 \le \frac{z}{a} < \frac{1}{2} \\ \frac{4}{3} - 4(\frac{z}{a}) + 4(\frac{z}{a})^2 - \frac{4}{3}(\frac{z}{a})^3 & \text{for } \frac{1}{2} \le \frac{z}{a} \le 1 \\ 0 & \text{otherwise.} \end{cases} \tag{18}$$

It can be verified that such φ_a gives a C^2 continuity. The correction coefficients $q_\alpha(\mathbf{x})$ are the coefficients of the monomials that vary with the location of approximation $\mathbf{x}$, which can be determined by the following reproducing conditions up to order p:

$$\sum_{I=1}^{N_s} \phi_I(\mathbf{x}) \mathbf{x}_I^\alpha = \mathbf{x}^\alpha, \quad |\alpha| \le p, \tag{19}$$

which leads to

$$\sum_{I=1}^{N_s} \phi_I(\mathbf{x}) \mathbf{H}(\mathbf{x} - \mathbf{x}_I) = \mathbf{H}(\mathbf{0}), \tag{20}$$

where $\mathbf{H}(\mathbf{x} - \mathbf{x}_I)$ is a column vector of the monomial bases

$$\mathbf{H}^T(\mathbf{x} - \mathbf{x}_I) = \left[(\mathbf{x} - \mathbf{x}_I)^\alpha \right]_{|\alpha| \le p}. \tag{21}$$

Combining (16), (17), and (20) reads

$$\phi_I(\mathbf{x}) = \mathbf{H}^T(\mathbf{0}) \mathbf{M}^{-1}(\mathbf{x}) \mathbf{H}(\mathbf{x} - \mathbf{x}_I) \varphi_a(||\mathbf{x} - \mathbf{x}_I||), \tag{22}$$

where $\mathbf{M}(\mathbf{x})$ is called the moment matrix defined as

$$\mathbf{M}(\mathbf{x}) = \sum_{I=1}^{N_s} \mathbf{H}(\mathbf{x}-\mathbf{x}_I)\mathbf{H}^T(\mathbf{x}-\mathbf{x}_I)\varphi_a(||\mathbf{x}-\mathbf{x}_I||). \tag{23}$$

By localization with reproducing kernel shape function, the condition number of the matrix $\mathbf{A}$ can be reduced from $O(\bar{h}^{-8})$ to $O(\bar{h}^{-2})$, compared with the RBF collocation method, with almost the same convergence behavior (Chen et al. 2008). However, when trying to solve nonlocal equations (1), the numerical test results in Sect. 5 indicate that it is not convergent. Therefore, we try to modify the scheme above, with the idea of requiring the localized RBF interpolation $u^h(\mathbf{x})$ to keep the reproducibility.

3.2 Improved localized RBF approximation with interpolation reproducibility

To achieve the interpolation reproducibility

$$v^h(\mathbf{x}) = v(\mathbf{x}), \quad v \in \mathbb{P}_p, \tag{24}$$

where $\mathbb{P}_p$ is the polynomial function space of degrees no more than p. Corresponding reproducing conditions can be defined as

$$\sum_{I=1}^{N_s} g_I(\mathbf{x})\phi_I(\mathbf{x})\mathbf{x}_I^\alpha = \mathbf{x}^\alpha, \quad |\alpha| \le p, \tag{25}$$

Follow (Pasetto et al. 2019), by the binomial theorem:

$$\begin{aligned}
\sum_{I=1}^{N_s} g_I(\mathbf{x})\phi_I(\mathbf{x})\,(\mathbf{x}-\mathbf{x}_I)^\alpha &= \sum_{I=1}^{N_s} g_I(\mathbf{x})\phi_I(\mathbf{x}) \prod_{p=1}^{d}\sum_{k_p=0}^{\alpha_p}\binom{\alpha_p}{k_p}(-1)^{k_p}x_p^{\alpha_p-k_p}x_{Ip}^{k_p} \\
&= \sum_{I=1}^{N_s} g_I(\mathbf{x})\phi_I(\mathbf{x}) \sum_{k_1=0}^{\alpha_1}\cdots\sum_{k_d=0}^{\alpha_d}\binom{\alpha_1}{k_1}\cdots\binom{\alpha_d}{k_d}(-1)^{|k|}\mathbf{x}^{\alpha-k}\mathbf{x}_I^k \\
&= \sum_{k_1=0}^{\alpha_1}\cdots\sum_{k_d=0}^{\alpha_d}\binom{\alpha_1}{k_1}\cdots\binom{\alpha_d}{k_d}(-1)^{|k|}\mathbf{x}^{\alpha-k}\sum_{I=1}^{N_s} g_I(x)\phi_I(\mathbf{x})\mathbf{x}_I^k \\
&= \sum_{k_1=0}^{\alpha_1}\cdots\sum_{k_d=0}^{\alpha_d}\binom{\alpha_1}{k_1}\cdots\binom{\alpha_d}{k_d}(-1)^{|k|}\mathbf{x}^{\alpha-k}\mathbf{x}^k \\
&= \mathbf{x}^\alpha\sum_{k_1=0}^{\alpha_1}\cdots\sum_{k_d=0}^{\alpha_d}\binom{\alpha_1}{k_1}\cdots\binom{\alpha_d}{k_d}(-1)^{|k|} \\
&= \mathbf{x}^\alpha\delta_{\alpha 0} = \delta_{\alpha 0},
\end{aligned} \tag{26}$$

where $\delta_{\alpha 0} = \delta_{\alpha_1 0}\delta_{\alpha_2 0}...\delta_{\alpha_d 0}$, and above reproducing condition means

$$\sum_{I=1}^{N_s} g_I(\mathbf{x})\phi_I(\mathbf{x})\mathbf{H}(\mathbf{x}-\mathbf{x}_I) = \mathbf{H}(\mathbf{0}), \tag{27}$$

which reads

$$\phi_I(\mathbf{x}) = \mathbf{H}^T(\mathbf{0})\mathbf{M}^{-1}(\mathbf{x})\mathbf{H}(\mathbf{x}-\mathbf{x}_I)\varphi_a(||\mathbf{x}-\mathbf{x}_I||), \tag{28}$$

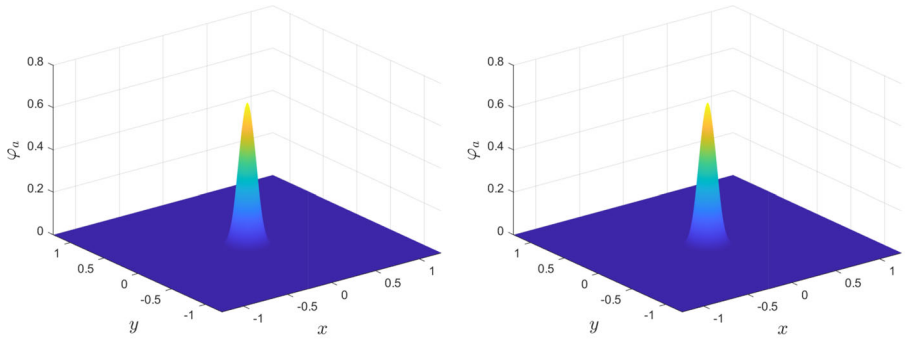

(a) Figure of kernel function (18) **(b)** Figure of localized RBF shape function (28)

Fig. 1 Kernel function and localized RBF shape function

where the moment matrix $\mathbf{M}$ of such modified method is defined as

$$\mathbf{M}(\mathbf{x}) = \sum_{I=1}^{N_s} g_I(\mathbf{x})\mathbf{H}(\mathbf{x}-\mathbf{x}_I)\mathbf{H}^T(\mathbf{x}-\mathbf{x}_I)\varphi_a(||\mathbf{x}-\mathbf{x}_I||). \tag{29}$$

One can compute the improved local shape function $\phi_I(\mathbf{x})$ by (28) and (29) straightforwardly. (b) of Fig. 1 shows the shape function using the improved localized RBF approximation. By numerical experiments in solving nonlocal diffusion equations, almost the same convergent behavior with RBF collocation methods will be shown with our modified local RBF collocation method, but the condition number of the coefficient matrix is significantly reduced as shown in Sect. 5, while the original RK localized RBF approximation is not convergent. In the next section, we will show more implement details using our method to deal with the nonlocal problems.

4 Solving nonlocal diffusion equations by modified local RBF method

Different from the classical differential operator, the nonlocal diffusion operator contained in (1) uses an integral operator as an alternative, so it needs more computational process in the discretization of such nonlocal integration.

Up to now, there have been a large number of works done for computing the nonlocal integration with finite interaction distance

$$I = \int_{B((x_0,y_0),\delta)} f(x,y)dxdy; \tag{30}$$

for instance, the one-point quadrature algorithms with partial areas (Seleson 2014). Such quadrature algorithms are easy to implement, while the accuracy is up to one. And the quadrature is based on integral reproducibility (Trask et al. 2019). It serves the collocation points as quadrature points, so it can be naturally used for damage modeling for peridynamics and can reach high accuracy. However, it needs great computational cost, since an optimization problem will be solved for every collocation point. And the fast algorithm based on fast multipole methods (Tian and Engquist 2019) leads to cheap computation cost, but it requires the mesh to have a hierarchical structure. In fact, computing such nonlocal integration effectively and efficiently is still an open problem. In this paper, we use the composite Gauss-type

quadrature rules mentioned in Pasetto et al. (2019), which are easy to use and can achieve relatively high accuracy.

Rewriting (30) using polar coordinates reads

$$I = \int_{B((x_0,y_0),\delta)} f(x,y)dxdy = \int_0^{\delta}\int_0^{2\pi} f(x_0 + r\cos\theta, y_0 + r\sin\theta)rd\theta dr. \quad (31)$$

By translating spherical neighborhood $B_{((x_0,y_0),\delta)}$ of point $\mathbf{x}_0 = (x_0, y_0)$ to a rectangular region $[0, 2\pi] \times [0, \delta]$, we can use the Gauss-type quadrature rules on such a region

$$\begin{aligned} I &= \int_{B((x_0,y_0),\delta)} f(x,y)dxdy = \int_0^{\delta}\int_0^{2\pi} f(x_0 + r\cos\theta, y_0 + r\sin\theta)rd\theta dr \\ &= \sum_g \omega_g f(x_0 + r_g\cos\theta_g, y_0 + r_g\sin\theta_g)r_g \\ &= \sum_g \tilde{\omega}_g f(x_g, y_g), \end{aligned} \quad (32)$$

where $x_g = x_0 + r_g\cos\theta_g$, $y_g = y_0 + r_g\sin\theta_g$ and $\tilde{\omega}_g = r_g\omega_g$. To archive higher accuracy, we use the composite Gauss-type quadrature by dividing the corresponding rectangular region into $m \times n$ subregions. The composite Gauss-type quadrature points in polar coordinates and corresponding cartesian coordinates after a polar coordinate transformation are shown in Fig. 2.

In this paper, we assume that $N_s = N_p = N$ and $\mathbf{T} = \mathbf{S}$, for the convenience of calculation and expression. Denoting $\{\mathbf{x}_1, \mathbf{x}_2, ..., \mathbf{x}_{N_I}\}$ the collocation points in inner domain Ω and $\{\mathbf{x}_{N_I+1}, \mathbf{x}_{N_I+2}, ..., \mathbf{x}_N\}$ the points on the interaction domain Ω_I. Substituting quadrature rules (32) into (1) reads

$$-\sum_{\mathbf{y}_g\in\mathcal{F}_I} \tilde{\omega}_g\rho_\delta(\mathbf{x}_I, \mathbf{y}_g)\sum_{J=1}^{N}(\phi_J(\mathbf{y}_g)g_J(\mathbf{y}_g) - \phi_J(\mathbf{x}_I)g_J(\mathbf{x}_I))u_J = f(\mathbf{x}_I), \quad \forall \mathbf{x}_I \in \mathbf{T}\cap\Omega, \quad (33)$$

where $\mathcal{F}_I$ means the set of composite Gauss-type quadrature points corresponding to $B(\mathbf{x}_I, \delta)$. And (33) can be rewritten as

$$\mathbf{Au} = \mathbf{b}; \quad (34)$$

the row of $\mathbf{A}$ which corresponding to $\mathbf{x}_I$ can be expressed as

$$\mathbf{A}_I^T = \begin{bmatrix} -\sum_{\mathbf{y}_g\in\mathcal{F}_I} \tilde{\omega}_g\rho_\delta(\mathbf{x}_I, \mathbf{y}_g)\left(\phi_1(\mathbf{y}_g)g_1(\mathbf{y}_g) - \phi_1(\mathbf{x}_I)g_1(\mathbf{x}_I)\right) \\ -\sum_{\mathbf{y}_g\in\mathcal{F}_I} \tilde{\omega}_g\rho_\delta(\mathbf{x}_I, \mathbf{y}_g)\left(\phi_2(\mathbf{y}_g)g_2(\mathbf{y}_g) - \phi_2(\mathbf{x}_I)g_2(\mathbf{x}_I)\right) \\ \cdots \\ -\sum_{\mathbf{y}_g\in\mathcal{F}_I} \tilde{\omega}_g\rho_\delta(\mathbf{x}_I, \mathbf{y}_g)\left(\phi_N(\mathbf{y}_g)g_N(\mathbf{y}_g) - \phi_N(\mathbf{x}_I)g_N(\mathbf{x}_I)\right) \end{bmatrix}, \quad (35)$$

and

$$\mathbf{u}^T = [u_1, u_2, ..., u_N], \quad (36)$$

and vector $\mathbf{b}$ can be expressed as

$$\mathbf{b}^T = [f(\mathbf{x}_1), f(\mathbf{x}_2), ..., f(\mathbf{x}_{N_I})]. \quad (37)$$

Fig. 2 Composite Gauss-type quadrature rules for nonlocal integration with finite interaction distance (2). **a** 4×4 composite Gauss-type quadrature points in polar coordinates. **b** 4×4 composite Gauss-type quadrature points in cartesian coordinates after a polar coordinate transformation

As for the Dirichlet volume constrains

$$u^h(\mathbf{x}_I) = \sum_{J=1}^{N} [\phi_J(\mathbf{x}_k) g_J(\mathbf{x}_k) u_J] = h(\mathbf{x}_k), \quad \forall \mathbf{x}_k \in \mathbf{T} \cap \Omega_I, \tag{38}$$

it can also be expressed as

$$\mathbf{Gu} = \mathbf{g}, \tag{39}$$

where the row of $\mathbf{G}$ which corresponds to $\mathbf{x}_k$ is

$$\mathbf{G}_k^T = \begin{bmatrix} \phi_1(\mathbf{x}_k) g_1(\mathbf{x}_k) \\ \phi_2(\mathbf{x}_k) g_2(\mathbf{x}_k) \\ \cdots \\ \phi_N(\mathbf{x}_k) g_N(\mathbf{x}_k) \end{bmatrix}, \tag{40}$$

and the vector $\mathbf{g}$ is

$$\mathbf{g}^T = [h(\mathbf{x}_{N_I+1}), h(\mathbf{x}_{N_I+2}), ..., h(\mathbf{x}_N)]. \tag{41}$$

By combining (34) and (39), the following linear equations can be derived:

$$\mathbf{Ku} = \mathbf{f}, \tag{42}$$

where

$$\mathbf{K}^T = [\mathbf{A}^T \ \mathbf{K}^T], \tag{43}$$

and

$$\mathbf{f}^T = [\mathbf{b}^T \ \mathbf{g}^T]. \tag{44}$$

Then, one can compute the coefficient vector $\mathbf{u}$ by solving (42).

5 Numerical experiments

We will investigate the convergence and the condition number of our improved localized RBF collocation method for solving nonlocal diffusion problem (1) with three numerical experiments, i.e., such a model with constant kernel, weak singular kernel, and strong singular kernel. Setting a two-dimensional domain $\Omega_\delta = [-1, 1] \times [-1, 1]$, which contains inner domain $\Omega = [-1 + \delta, 1 - \delta] \times [-1 + \delta, 1 - \delta]$ and boundary layer $\Omega_I = \Omega_\delta \backslash \Omega$ (see Fig. 3). Before solving, we briefly introduce some notations used in the numerical results. The label RBF, RBF RK1, RBF RK2 means the RBF collocation method, RK-enhanced localized RBF collocation method in Chen et al. (2008), and our improved localized RBF collocation method, respectively.

For the convenience of computation, we use a uniform grid as Fig. 4,

with the grid distance $\bar{h}_x = \bar{h}_y = \frac{2}{N_1}$, where N_1 is the number of cells divided in one direction of the domain Ω_δ.

5.1 Nonlocal diffusion problem with constant kernel

We choose an exact solution $u(x, y) = \sin(x)\cos(y)$, and consider a constant kernel first

$$\rho_\delta(\mathbf{x}, \mathbf{y}) = \frac{4}{\pi \delta^4}. \tag{45}$$

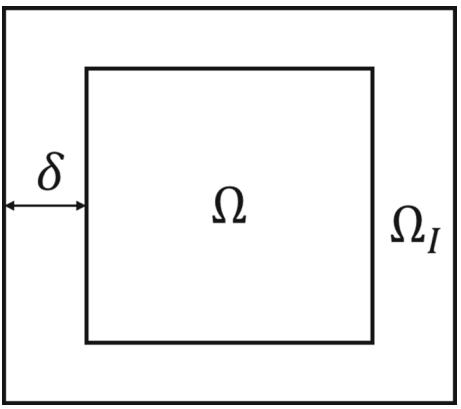

Fig. 3 The computational domain

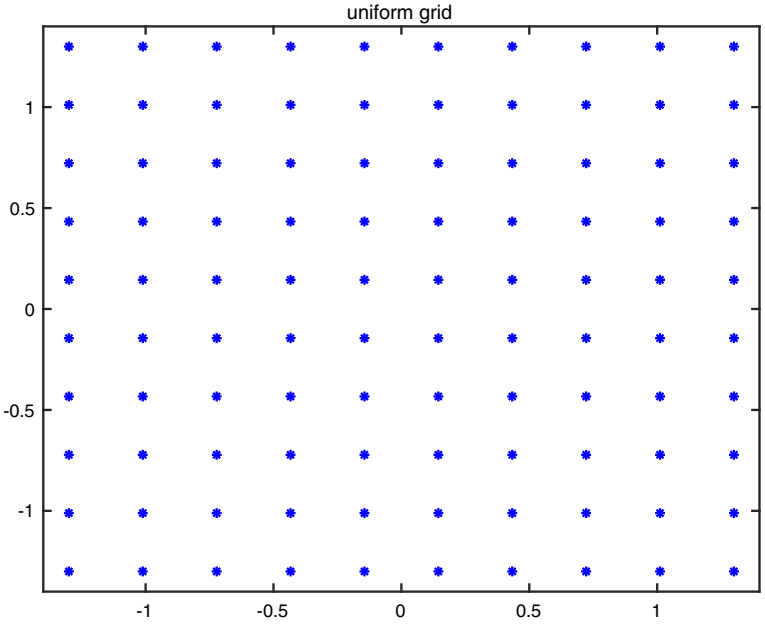

Fig. 4 The uniform grid to discrete the computational domain

One can easily justify that such kernel meets the condition (4). Setting $\bar{h}_x = \bar{h}_y = h$ and we start with $N_1 = 8$ and choosing RBF shape parameter $c = h, 2h, 3h$. We choose $\delta = 3.01\ h$ to avoid the possible wrong judgement of the positional relationship between point $\mathbf{x}_J$ and $B_{(\mathbf{x}_I,\delta)}$ caused by rounding error when using $\delta = 3\ h,$ and the error L^2 norm can be computed by the composite Gauss-quadrature rules

$$||u - u^h||_{L^2_\Omega} = \left[\int_\Omega \left(u^h(\mathbf{x}) - u(\mathbf{x})\right)^2\right]^{\frac{1}{2}} \approx \left[\sum_{n_e=1}^{N_e}\sum_{g=1}^{n_g}\left(u^h(\mathbf{x}_g^{n_e}) - u(\mathbf{x}_g^{n_e})\right)^2 \omega_g^{n_e}\right]^{\frac{1}{2}}, \quad (46)$$

where N_e is the number of elements which are used to discrete Ω, and we choose the uniform triangle elements during the implementation to compute the numerical quadrature in (46). We

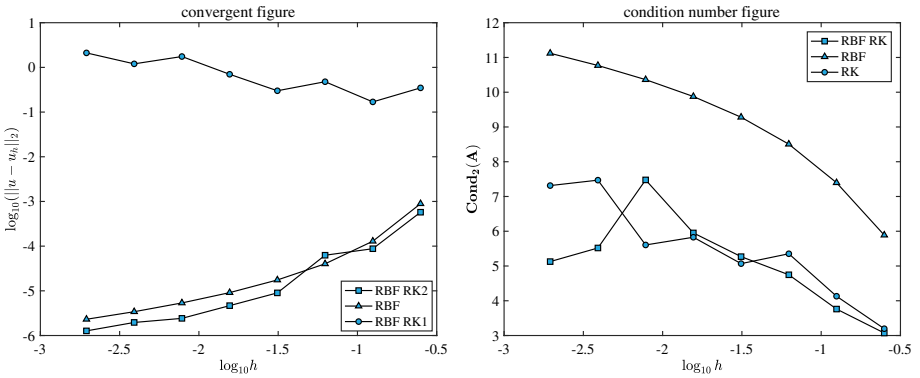

Fig. 5 Convergence study (**a**) and condition number study (**b**) with $\delta = 3.01h$, $a = 3.01h$, $c = h$, and $\rho_\delta = \frac{4}{\pi\delta^4}$

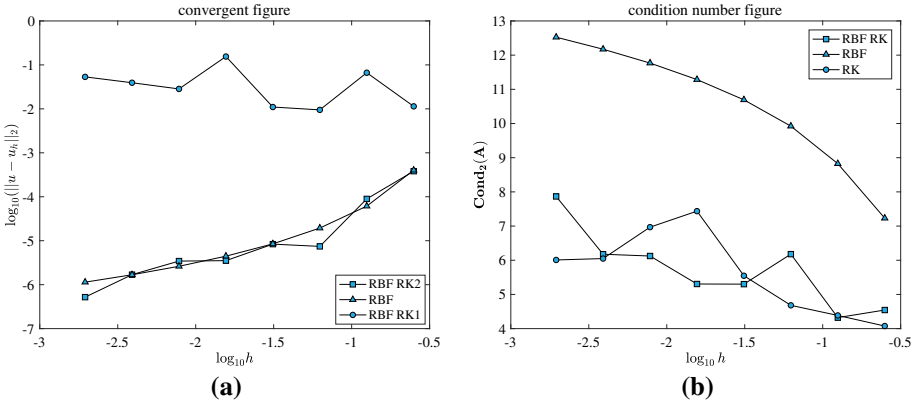

Fig. 6 Convergence study (**a**) and condition number study (**b**) with $\delta = 3.01h$, $a = 3.01h$, $c = 2h$, and $\rho_\delta = \frac{4}{\pi\delta^4}$

remark that the elements here are only used to compute the L^2 error norm in the numerical examples. And there are no need to use elements to solve the nonlocal equations. $\mathbf{x}_g^{n_e}$ and $\omega_g^{n_e}$ denote the Gauss-quadrature point and weight in n_e^{th} element, respectively. Corresponding convergences and condition numbers results with the refinement of discretization are shown in Figs. 5, 6, 7 and Tables 1, 2, 3. It can be found that our improved localized RBF collocation method converges as fast as the RBF method, while the condition number and the time-consuming for assembly of the stiffness matrix are much smaller than it, while the method mentioned in Chen et al. (2008) is not convergent for nonlocal diffusion problems. In the next subsection, we will try to solve nonlocal problems with the singular kernels.

Table 1 Convergence and condition number results with $\delta = 3.01h$, $a = 3.01h$, $c = h$, and $\rho_\delta = \frac{4}{\pi\delta^4}$

N_1	RBF			RBF RK1 Chen et al. (2008)			RBF RK2		
	$\|\|u-u^h\|\|_{L^2_\Omega}$	$\text{Cond}_2(\mathbf{A})$	Times	$\|\|u-u^h\|\|_{L^2_\Omega}$	$\text{Cond}_2(\mathbf{A})$	Times	$\|\|u-u^h\|\|_{L^2_\Omega}$	$\text{Cond}_2(\mathbf{A})$	Times
8	8.9137*e*−04	7.7444*e*+05	1.50	3.4824*e*−01	1.5691*e*+03	2.42	5.7356*e*−04	1.1776e+03	3.67
16	1.2867*e*−04	2.4982*e*+07	59.16	1.6991*e*−01	1.3454*e*+04	26.39	8.7646*e*−05	5.7657e+03	28.42
24	4.0201*e*−05	3.2026*e*+08	525.58	4.7829*e*−01	2.2450*e*+05	105.31	6.2458*e*−05	5.5894e+04	96.14
32	1.7478*e*−05	1.9099*e*+09	1750.82	3.0012*e*−01	1.1734*e*+05	218.19	9.0042*e*−06	1.8585e+05	217.56
40	9.1292*e*−06	7.5305*e*+09	4533.06	7.0143*e*−01	6.7160*e*+05	381.45	2.6557*e*−05	8.9517e+05	460.97
48	5.3605*e*−06	2.2966*e*+10	10887.41	1.7532*e*+00	4.0256*e*+05	728.31	2.4190*e*−06	2.9984*e*+07	705.20
56	3.4137*e*−06	5.8770*e*+10	18253.65	1.2072*e*+01	2.9450*e*+07	1073.67	1.9765*e*−06	3.2988*e*+05	1047.13
64	2.3076*e*−06	1.3238*e*+11	36362.84	2.1075*e*+00	2.0613*e*+07	1503.52	1.4753*e*−06	1.3389*e*+06	1580.22

Table 2 Convergence and condition number results with $\delta = 3.01h$, $a = 3.01h$, $c = 2h$, and $\rho_\delta = \frac{4}{\pi\delta^4}$

N_1	RBF			RBF RK1 Chen et al. (2008)			RBF RK2		
	$\|\|u-u^h\|\|_{L^2_\Omega}$	$\text{Cond}_2(\mathbf{A})$	Times	$\|\|u-u^h\|\|_{L^2_\Omega}$	$\text{Cond}_2(\mathbf{A})$	Times	$\|\|u-u^h\|\|_{L^2_\Omega}$	$\text{Cond}_2(\mathbf{A})$	Times
8	4.0190$e-$04	1.6963e+07	1.82	1.1429$e-$02	1.1883e+04	2.21	3.8240$e-$04	3.5029e+04	2.32
16	6.1182$e-$05	6.6898e+08	45.90	6.6459$e-$02	2.4346e+04	25.90	8.9414$e-$05	2.1008e+04	23.15
24	1.9362$e-$05	8.3703e+09	498.24	9.4791$e-$03	4.8034e+04	99.46	7.4284$e-$06	1.5108e+06	100.58
32	8.4797$e-$06	4.9347e+10	1782.43	1.1037$e-$02	3.5234e+05	221.42	8.3630$e-$06	2.0002e+05	212.63
40	4.4517$e-$06	1.9313e+11	4601.97	1.5529$e-$01	2.7343e+07	374.92	2.5152$e-$06	2.0281e+05	439.80
48	2.6238$e-$06	5.8577e+11	10756.21	2.8366$e-$02	9.2851e+06	715.37	4.4442$e-$06	1.3270e+06	701.99
56	1.6758$e-$06	1.4926e+12	18337.39	3.9292$e-$02	1.1160e+06	1085.68	1.6942$e-$06	1.4988e+06	1053.27
64	1.1355e-06	3.3506e+12	36252.88	5.3707e-02	1.0244e+06	1576.90	5.2032$e-$07	7.3380e+07	1502.51

Table 3 Convergence and condition number results with $\delta = 3.01h$, $a = 3.01h$, $c = 3h$, and $\rho_\delta = \frac{4}{\pi\delta^4}$

N_1	RBF			RBF RK1 Chen et al. (2008)			RBF RK2		
	$\|\|u-u^h\|\|_{L^2_\Omega}$	$\text{Cond}_2(\mathbf{A})$	Times	$\|\|u-u^h\|\|_{L^2_\Omega}$	$\text{Cond}_2(\mathbf{A})$	Times	$\|\|u-u^h\|\|_{L^2_\Omega}$	$\text{Cond}_2(\mathbf{A})$	Times
8	1.6498*e*−04	5.4893*e*+08	1.14	6.2660*e*−02	1.6340*e*+05	2.89	6.3899*e*−04	9.9801*e*+03	3.95
16	2.6672*e*−05	2.6260*e*+10	63.26	1.0475*e*−03	3.6264*e*+04	27.91	1.2365*e*−05	2.4801*e*+05	28.81
24	8.5583*e*−06	3.3904*e*+11	493.64	1.2653*e*−03	1.2825*e*+05	95.93	7.6151*e*−06	2.8075*e*+05	95.20
32	3.7738*e*−06	2.0259*e*+12	1784.09	2.2411*e*−03	1.0925*e*+05	231.08	1.5762*e*−06	2.6519*e*+05	225.79
40	1.9903*e*−06	7.9822*e*+12	4597.65	3.6976*e*−03	4.3068*e*+05	402.06	1.0584*e*−06	2.8013*e*+06	448.16
48	1.1771*e*−06	2.4301*e*+13	10921.14	5.5948*e*−03	1.1286*e*+06	733.48	5.1735*e*−07	2.0721*e*+06	732.51
56	7.5385*e*−07	6.2064*e*+13	18141.76	7.9140*e*−03	4.2533*e*+05	1043,87	3.8419*e*−07	1.4018*e*+06	1082.79
64	5.1192*e*−07	1.3953*e*+14	36501.23	1.0663*e*−02	8.9734*e*+06	1496.50	2.3137*e*−07	1.3515*e*+06	1492.08

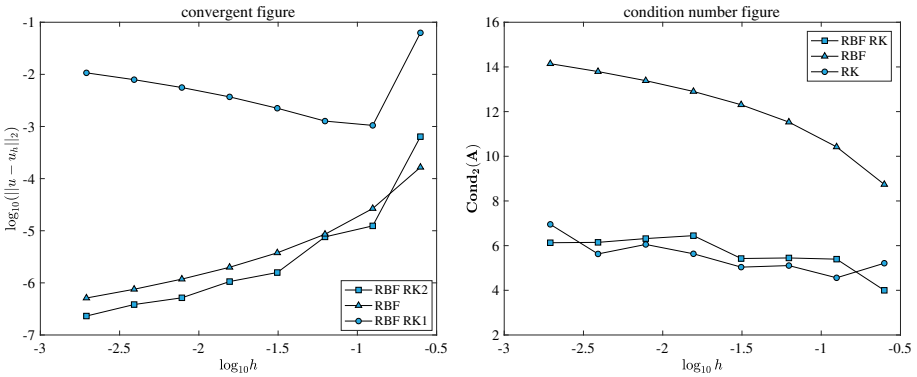

Fig. 7 Convergence study (**a**) and condition number study (**b**) with $\delta = 3.01h$, $a = 3.01h$, with $c = 3h$, and $\rho_\delta = \frac{4}{\pi\delta^4}$

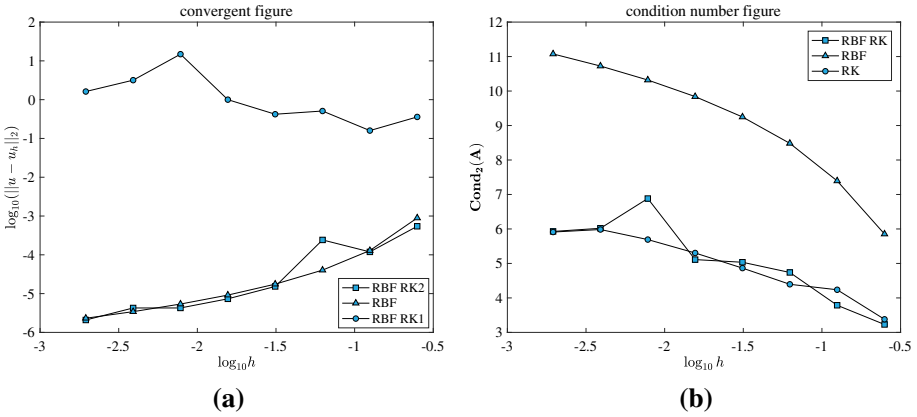

Fig. 8 Convergence study (**a**) and condition number study (**b**) with $\delta = 3.01h$, $a = 3.01h$, $c = h$, and $\rho_\delta = \frac{7}{\pi\delta^{7/2}} \frac{1}{||\mathbf{x}-\mathbf{y}||^{1/2}}$

5.2 Nonlocal diffusion problem with singular kernels

In this subsection, we will test our localized RBF method by solving a nonlocal diffusion problem with a singular kernel. First, we set the kernel function $\rho_\delta(\mathbf{x}, \mathbf{y})$ as follows:

$$\rho_\delta(\mathbf{x}, \mathbf{y}) = \frac{7}{\pi\delta^{7/2}} \frac{1}{||\mathbf{x}-\mathbf{y}||^{1/2}}, \tag{47}$$

and one can also easily verify that such kernel function (47) has a bounded second-order moment (4). It shows by our numerical tests that the localized RBF collocation developed in this paper has almost the same convergent behavior compared with RBF collocation methods, even for the kernel with weak singularity. The corresponding results will be shown in Figs. 8, 9, 10 and Tables 4, 5, 6.

Now, let us test our method for the kernel with strong singularity. As mentioned in Witman et al. (2016), the convergent rate will decrease if we simply use the finite-element method to

Table 4 Convergence and condition number results with $\delta = 3.01h$, $a = 3.01h$, $c = h$, and $\rho_\delta = \frac{7}{\pi\delta^{7/2}}\frac{1}{||\mathbf{x}-\mathbf{y}||^{1/2}}$

N_1	RBF			RBF RK1 Chen et al. (2008)			RBF RK2		
	$\|\|u-u^h\|\|_{L^2_\Omega}$	$\text{Cond}_2(\mathbf{A})$	Times	$\|\|u-u^h\|\|_{L^2_\Omega}$	$\text{Cond}_2(\mathbf{A})$	Times	$\|\|u-u^h\|\|_{L^2_\Omega}$	$\text{Cond}_2(\mathbf{A})$	Times
8	8.9162e−04	7.1336e+05	1.39	3.5866e−01	2.3958e+03	2.59	5.4433e−04	1.6955e+03	2.86
16	1.2886e−04	2.4781e+07	62.01	1.5950e−01	1.7237e+04	23.70	1.1932e−04	6.1191e+03	29.14
24	4.0295e−05	3.0402e+08	512.27	5.0972e−01	2.4830e+04	100.21	2.4196e−04	5.4690e+04	108.62
32	1.7528e−05	1.7729e+09	1790.20	4.2113e−01	7.3190e+04	225.80	1.5268e−05	1.0819e+05	203.58
40	9.1593e−06	6.9017e+09	4509.83	1.0026e+00	2.0094e+05	393.17	7.3363e−06	1.2927e+05	424.07
48	5.3799e−06	2.0871e+10	10841.16	1.4866e+01	4.9245e+05	719.62	4.2664e−06	7.6344e+06	711.29
56	3.4270e−06	5.3086e+10	18254.98	3.1789e+00	9.6282e+05	1032.16	4.2737e−06	1.0465e+06	1105.69
64	2.3171e−06	1.1903e+11	35891.71	1.6187e+00	8.1439e+05	1538.75	2.0874e−06	8.4716e+05	1552.64

Table 5 Convergence and condition number results with $\delta = 3.01h$, $a = 3.01h$, $c = 2h$, and $\rho_\delta = \frac{7}{\pi\delta^{7/2}}\frac{1}{||\mathbf{x}-\mathbf{y}||^{1/2}}$

N_1	RBF			RBF RK1 Chen et al. (2008)			RBF RK2		
	$\|\|u-u^h\|\|_{L^2_\Omega}$	$\text{Cond}_2(\mathbf{A})$	Times	$\|\|u-u^h\|\|_{L^2_\Omega}$	$\text{Cond}_2(\mathbf{A})$	Times	$\|\|u-u^h\|\|_{L^2_\Omega}$	$\text{Cond}_2(\mathbf{A})$	Times
8	4.0190e−04	1.6963e+07	1.91	1.4282e−02	9.2649e+03	2.88	3.8152e−04	9.5820e+04	3.00
16	6.1182e−05	6.6898e+08	56.08	6.5964e−02	2.9270e+04	22.89	9.9353e−05	2.4492e+04	21.23
24	1.9362e−05	8.3703e+09	534.70	1.0576e−02	4.4902e+04	102.53	7.4788e−06	3.9587e+06	104.07
32	8.4797e−06	4.9347e+10	1736.44	1.2172e−02	1.4764e+05	227.52	7.3710e−06	1.3862e+05	214.08
40	4.4517e−06	1.9313e+11	4608.59	2.0238e−02	1.3096e+06	397.61	3.5525e−06	2.0609e+05	400.15
48	2.6238e−06	5.8577e+11	10783.35	3.1343e−02	1.1934e+06	733.20	1.6283e−06	1.2266e+07	784.29
56	1.6758e−06	1.4926e+12	18360.62	4.4203e−02	4.3136e+05	1115.27	1.1875e−06	4.8499e+06	1043.92
64	1.1355e−06	3.3506e+12	16189.48	6.6065e−02	9.0612e+05	1542.61	5.6570e−07	1.0952e+07	1602.61

Table 6 Convergence and condition number results with $\delta = 3.01h$, $a = 3.01h$, $c = 3h$, and $\rho_\delta = \frac{7}{\pi\delta^{7/2}}\frac{1}{||\mathbf{x}-\mathbf{y}||^{1/2}}$

N_1	RBF			RBF RK1 Chen et al. (2008)			RBF RK2		
	$\|\|u-u^h\|\|_{L^2_\Omega}$	$\text{Cond}_2(\mathbf{A})$	Times	$\|\|u-u^h\|\|_{L^2_\Omega}$	$\text{Cond}_2(\mathbf{A})$	Times	$\|\|u-u^h\|\|_{L^2_\Omega}$	$\text{Cond}_2(\mathbf{A})$	Times
8	1.6498e−04	5.4893e+08	1.32	1.5909e−02	2.3266e+05	3.17	7.1235e−04	1.0673e+04	3.39
16	2.6672e−05	2.6260e+10	53.30	1.0562e−03	3.4944e+04	28.69	1.2420e−05	5.6283e+05	25.56
24	8.5583e−06	3.3904e+11	530.83	1.3562e−03	3.0734e+05	109.03	7.7568e−06	3.0012e+05	97.22
32	3.7738e−06	2.0259e+12	1864.09	2.4613e−03	1.3312e+05	202.97	1.7529e−06	2.6259e+06	239.20
40	1.9903e−06	7.9822e+12	4520.74	4.1053e−03	9.9695e+07	425.16	7.7231e−07	4.7537e+05	441.62
48	1.1771e−06	2.4301e+13	10842.75	6.2373e−03	8.1050e+05	731.44	5.8747e−07	7.8142e+05	690.47
56	7.5385e−07	6.2064e+13	18298.73	8.8485e−03	8.7772e+05	1104.28	9.7806e−07	9.6489e+06	1079.21
64	5.1192e−07	1.3953e+14	36278.10	1.1945e−02	7.6285e+06	1573.41	2.5115e−07	1.8398e+06	1596.74

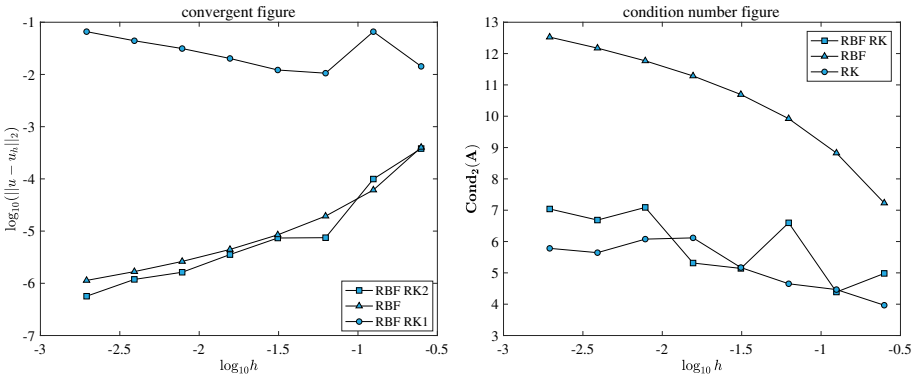

Fig. 9 Convergence study (**a**) and condition number study (**b**) with $\delta = 3.01h$, $a = 3.01h$, $c = 2h$, and $\rho_\delta = \frac{7}{\pi\delta^{7/2}}\frac{1}{||\mathbf{x}-\mathbf{y}||^{1/2}}$

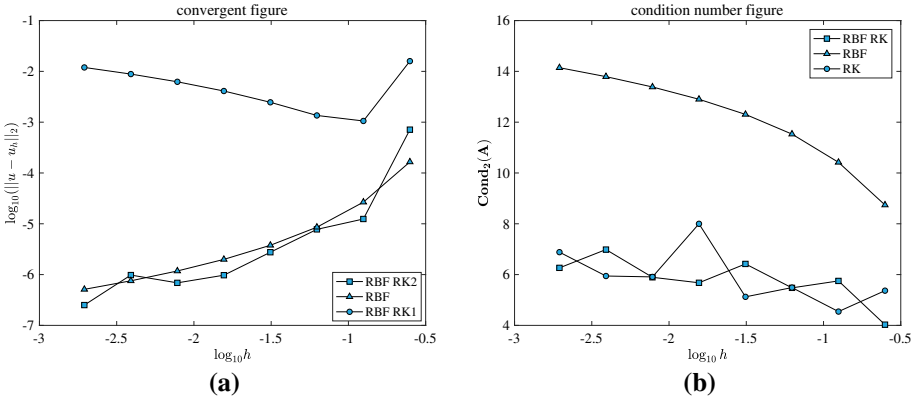

Fig. 10 Convergence study (**a**) and condition number study (**b**) with $\delta = 3.01h$, $a = 3.01h$, $c = 3h$, and $\rho_\delta = \frac{7}{\pi\delta^{7/2}}\frac{1}{||\mathbf{x}-\mathbf{y}||^{1/2}}$

solve nonlocal problems with strong singular kernels. Here, we take the kernel function with strong singularity, for the problem (1)

$$\rho_\delta(\mathbf{x},\mathbf{y}) = \frac{4}{\pi\delta^2}\frac{1}{||\mathbf{x}-\mathbf{y}||^2}. \tag{48}$$

The following numerical result in Fig. 11 and Table 7 shows that our localized RBF collocation method holds almost the same convergence behavior compared with the RBF collocation method, even for the kernel with strong singularity.

6 Conclusion

In this work, we have proposed a new localized RBF interpolation approximation with reproducibility for nonlocal diffusion problems. The key idea was to modify the reproducing kernel

Table 7 Convergence and condition number results with $\delta = 3.01h$, $a = 3.01h$, $c = 3h$, $c = 4h$, and $\rho_\delta = \frac{4}{\pi\delta^2}\frac{1}{||\mathbf{x}-\mathbf{y}||^2}$

N_1	RBF($c = 3h$)		RBF($c = 4h$)		RBF RK2($c = 3h$)		RBF RK2($c = 4h$)	
	$\|\|u - u^h\|\|_{L^2_\Omega}$	$\text{Cond}_2(\mathbf{A})$	$\|\|u - u^h\|\|_{L^2_\Omega}$	$\text{Cond}_2(\mathbf{A})$	$\|\|u - u^h\|\|_{L^2_\Omega}$	$\text{Cond}_2(\mathbf{A})$	$\|\|u - u^h\|\|_{L^2_\Omega}$	$\text{Cond}_2(\mathbf{A})$
8	1.6498$e-$04	5.4893e+08	6.6508$e-$05	1.8706e+10	9.0812$e-$04	3.8267e+04	1.4237$e-$04	7.1915e+03
16	2.6672$e-$05	2.6260e+10	1.1354$e-$05	1.2077e+12	1.3335$e-$05	1.9983e+06	2.0307$e-$05	1.7265e+06
24	8.5583$e-$06	3.3904e+11	3.7058$e-$06	1.6382e+13	6.3418$e-$06	3.7985e+06	3.7616$e-$06	1.0810e+08
32	3.7738$e-$06	2.0259e+12	1.6458$e-$06	9.9654e+13	2.3312$e-$06	6.1842e+06	1.5537$e-$06	2.6038e+07
40	1.9903$e-$06	7.9822e+12	8.7190$e-$07	3.9593e+14	1.2954$e-$06	6.6485e+06	8.3547$e-$07	1.1104e+08
48	1.1771$e-$06	2.4301e+13	5.1437$e-$07	1.2112e+15	1.5333$e-$06	5.9237e+09	5.7343$e-$07	3.1119e+08
56	7.5385$e-$07	6.2064e+13	3.3216$e-$07	3.1022e+15	7.4068$e-$07	5.8574e+08	3.9720e-07	1.3631e+10
64	5.1192$e-$07	1.3953e+14	2.2603$e-$07	6.9615e+15	5.1492$e-$07	1.6367e+09	3.1313$e-$07	2.2931e+09

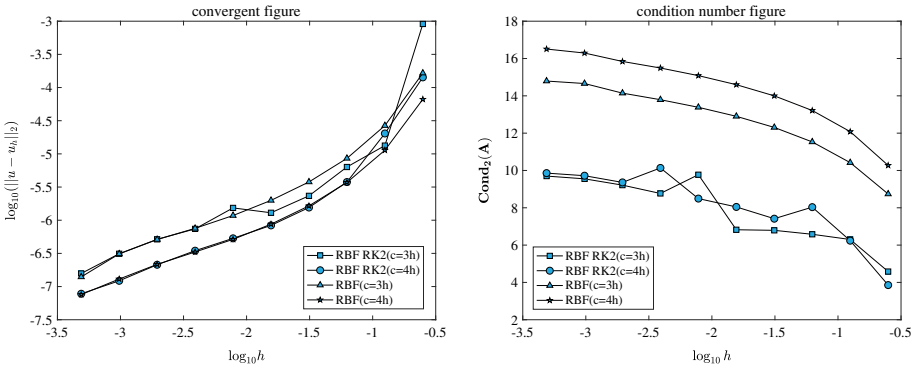

Fig. 11 Convergence study (**a**) and condition number study (**b**) with $\delta = 3.01h$, $a = 3.01h$, $c = 3h$, $c = 4h$, and $\rho_\delta = \frac{4}{\pi\delta^2}\frac{1}{||\mathbf{x}-\mathbf{y}||^2}$

localized RBF method in Chen et al. (2008) by redesigning the reproducing condition, which allows the interpolation function $u^h(\mathbf{x})$ to meet the reproducibility. Three types of numerical results indicate that it offers almost the same convergence behavior, but is better conditioned and time-saving compared with RBF collocation methods. Compared with the fact that the method in Chen et al. (2008) is not convergent for the nonlocal diffusion problem, our improved localized RBF collocation achieves a high convergence rate for such equations. Even for the nonlocal problem with a strong singular kernel which cannot be handled well by finite-element methods, our localized RBF method is also effective. As for the discretization of the nonlocal integration, the composite Gauss-type quadrature rules are still valid for our method.

Acknowledgements This research was supported by National Natural Science Foundation of China (No. 11971386) and the National Key R&D Program of China (No. 2020YFA0713603).

References

Alali B, Albin N (2020) Fourier spectral methods for nonlocal models. J Peridyn Nonlocal Model 2:317–335
Ali SV, Alfa H, Elisabeth L (2015) A radial basis function partition of unity collocation method for convection–diffusion equations arising in financial applications. J Sci Comput 64(2):341–367
Buhmann MD (2003) Radial basis functions: theory and implementations. Cambridge University Press, Cambridge
Chen JS, Hu W, Hu HY (2008) Reproducing kernel enhanced local radial basis collocation method. Int J Numer Meth Eng 75(5):600–627
D'Elta M, Gunzburger M, Vollmann CA (2020) Cookbook for finite element methods for nonlocal problems, including quadrature rules and approximate Euclidean balls, arXiv:2005.10775
Du Q, Yin XB (2018) A conforming DG method for linear nonlocal models with integrable kernels. J Sci Comput 80:1913–1935
Du Q, Gunzburger M, Lehoucq RB, Zhou K (2012) Analysis and approximation of nonlocal diffusion problems with volume constraints. SIAM Rev 54(4):667–696
Du Q, Huang Z, Lehoucq RB (2014) Nonlocal convection-diffusion volume-constrained problems and jump processes. Discrete Contin Dyn Syst 19(2):373–389
Du Q, Ju LL, Lu JF (2018) A discontinuous Galerkin method for one-dimensional time-dependent nonlocal diffusion problems. Math Comput 88(315):123–147

Du N, Sun HW, Wang H (2019) A preconditioned fast finite difference scheme for space-fractional diffusion equations in convex domains. Comput Appl Math 38(14). https://doi.org/10.1007/s40314-019-0769-9
Hu YT, Li ZC, Cheng HD (2005) Radial basis collocation methods for elliptic boundary value problems. Comput Math Appl 50(1–2):289–320
Leng Y, Tian XC, Trask NA, Foster JT (2020) Asymptotically compatible reproducing kernel collocation and meshfree integration for the peridynamic Navier equation. Comput Methods Appl Mech Eng 370:113264. https://doi.org/10.1016/j.cma.2020.113264
Liu WK, Jun S, Zhang YF (1995) Reproducing kernel particle methods. Int J Numer Meth Fluids 20:1081–1106
Liu WK, Chen Y, Jun S, Chen JS, Chang CT (1996) Overview and applications of the reproducing kernel particle methods. Arch Comput Methods Eng 3(1):3–80
Liu H, Cheng AJ, Wang H (2018) A fast discontinuous galerkin method for a bond-based linear peridynamic model discretized on a locally refined composite mesh. J Sci Comput 76:913–942
Madych WR, Nelson SA (1990) Multivariate interpolation and conditionally positive definite functions. II. Math Comput 54(189):211–230
Madych WR, Nelson SA (1992) Bounds on multivariate polynomials and exponential error estimates for multiquadric interpolation. J Approx Theory 70(1):94–114
Metzler R, Klafter J (2000) The random walk's guide to anomalous diffusion: a fractional dynamics approach. Phys Rep 339(1):1–77
Pasetto M, Leng Y, Chen JS, Foster, Seleson P (2019) A reproducing kernel enhanced approach for peridynamic solutions. Comput Methods Appl Mech Eng 340(Oct. 1):1044–1078
Perracchione E (2018) Rational RBF-based partition of unity method for efficiently and accurately approximating 3D objects. Comput Appl Math 37:4633–4648
Seleson P (2014) Improved one-point quadrature algorithms for two-dimensional peridynamic models based on analytical calculations. Comput Methods Appl Mech Eng 282(dec.1):184–217
Silling SA (2000) Reformulation of elasticity theory for discontinuities and long-range forces. J Mech Phys Solids 48(1):175–209
Tian XC, Engquist B (2019) Fast algorithm for computing nonlocal operators with finite interaction distance. Commun Math Sci 17(6):1653–1670
Trask N, You HQ, Yu Y, Parks ML (2019) An asymptotically compatible meshfree quadrature rule for nonlocal problems with applications to peridynamics. Comput Methods Appl Mech Eng 343:151–165
Witman DR, Gunzburger M, Peterson J (2016) Reduced-order modeling for nonlocal diffusion problems. Int J Numer Meth Fluids 83(3):307–327
Zhang SY, Nie YF (2020) A POD-Based fast algorithm for the nonlocal unsteady problems. Int J Numer Anal Model 17(6):858–871